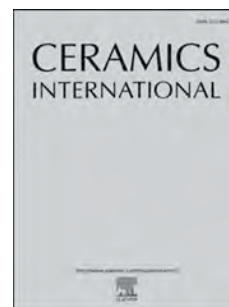


Journal Pre-proof

Synthesis of LiBGeO_4 using compositional design and its dielectric behaviors at RF and microwave frequencies

Zhuo Xing, Changzhi Yin, Zezong Yu, Jibran Khaliq, Chunchun Li



PII: S0272-8842(20)31650-3

DOI: <https://doi.org/10.1016/j.ceramint.2020.06.004>

Reference: CERI 25431

To appear in: *Ceramics International*

Received Date: 7 May 2020

Revised Date: 26 May 2020

Accepted Date: 1 June 2020

Please cite this article as: Z. Xing, C. Yin, Z. Yu, J. Khaliq, C. Li, Synthesis of LiBGeO_4 using compositional design and its dielectric behaviors at RF and microwave frequencies, *Ceramics International* (2020), doi: <https://doi.org/10.1016/j.ceramint.2020.06.004>.

This is a PDF file of an article that has undergone enhancements after acceptance, such as the addition of a cover page and metadata, and formatting for readability, but it is not yet the definitive version of record. This version will undergo additional copyediting, typesetting and review before it is published in its final form, but we are providing this version to give early visibility of the article. Please note that, during the production process, errors may be discovered which could affect the content, and all legal disclaimers that apply to the journal pertain.

© 2020 Published by Elsevier Ltd.

Synthesis of LiBGeO₄ using compositional design and its dielectric behaviors at RF and microwave frequencies

Zhuo Xing¹, Changzhi Yin², Zezong Yu³, Jibran Khaliq^{4*}, Chunchun Li^{2, 3*}

¹*School of Electronic Information Engineering, Xijing University, Xi'an 710123, China*

²*College of Information Science and Engineering, Guilin University of Technology, Guilin, 541004, China*

³*School of Materials Science and Engineering, Nanchang University, Nanchang 330031, People's Republic of China*

⁴*Department of Mechanical and Construction Engineering, Faculty of Engineering and Environment, Northumbria University at Newcastle, NE1 8ST, UK*

Abstract

Borates are promising candidates as dielectric substrate materials in low temperature cofired ceramics technology (LTCC) due to their relative low sintering temperatures and relative permittivities compared to their counterparts. However, synthesizing borates having single-phase is still challenging because of the volatility and hydrophilicity of boron resources. In this work, a compositional design was utilized to synthesize single-phase LiBGeO₄ ceramics over a broad temperature range from 600 to 840 °C. Radio-frequency dielectric behaviours featured a strong temperature dependence, especially at high temperatures (> 400 °C), which is related to the thermally activated polarizations. LiBGeO₄ ceramic sintered at 820 °C has optimum microwave dielectric properties with the relative permittivity (ϵ_r) of 6.28, a quality factor ($Q \times f$) of 21,620 GHz, and a temperature coefficient of resonance frequency (τ_f) of -88.7 ppm/°C. LiBGeO₄ also showed chemical inertness when cofired with silver (Ag), provided an evidence for its utilization in LTCC technology. Overall, this work provides a strategy for facile synthesis of phase pure borates, via the proposed two-step process to obtain stable boron resources.

Keywords: Precursor synthesis; Dielectric properties; Ceramics; Borates; LiBGeO₄

* Authors to whom correspondence should be addressed: jibran.khaliq@northumbria.ac.uk; lichunchun2003@126.com

1. Introduction

With the recent commercialization and adaptation of 5G, microwave dielectric materials have witnessed accelerated progress towards miniaturization for high-permittivity materials and exploration of low-permittivity materials for fast signal propagation [1-2]. Low-temperature co-fired ceramics (LTCC) technology has an ability to integrate various passive microwave components like resonators, capacitors, filters, and antennas, etc [3-5]. It is expected that LTCC can achieve miniaturization and high data transmission speed simultaneously by laminating low-permittivity candidates to form 3D modules. One of the conditions for these LTCC is to have relatively low sintering temperatures ($< 960\text{ }^{\circ}\text{C}$), as the ceramics can be cofired with the commonly used inner metal electrodes such as Ag (melting temperature $961\text{ }^{\circ}\text{C}$), without having a chemical reaction. High quality factors ($Q \times f$) and temperature stability of the resonance frequency should be fulfilled [6-9].

Generally, the use of glass or addition of sintering aids are recognized as compelling strategies for reducing sintering temperature [10, 11]. However, these methods usually cause deterioration of the dielectric properties (especially the quality factor) as the residual and aggregated glasses or sintering aids act as second phases which leads to additional interfaces [12, 13]. Recently, ceramics with intrinsic low densification temperatures, e.g. $\text{Li}_2\text{O-M}_2\text{O}_5\text{-TiO}_2$ ($\text{M} = \text{Nb, Ta}$) system and $\text{Bi}_2\text{O}_3\text{-TeO}_2$ system, have been widely explored, which opened a new stage for LTCC technology [14, 15]. Until now, numerous ceramics that could be densified at temperatures lower than $960\text{ }^{\circ}\text{C}$ have been developed [16, 17], consisting mainly of low-melting-point constituents, such as B_2O_3 ($450\text{ }^{\circ}\text{C}$), Bi_2O_3 ($824\text{ }^{\circ}\text{C}$), MoO_3 ($795\text{ }^{\circ}\text{C}$), and V_2O_5 ($690\text{ }^{\circ}\text{C}$), etc [18-23]. Amongst them, borates exhibit extremely low densification temperatures ($< 700\text{ }^{\circ}\text{C}$) and ultra-low relative permittivities (e.g. $\epsilon_r = 4.2$ for $\text{Li}_3\text{AlB}_2\text{O}_6$, and $\epsilon_r = 4.2$ for H_3BO_3) because of the low ionic polarizability of B^{3+} (0.05 \AA),

making them excellent candidates for ultra-low temperature co-fired ceramics (ULTCC) [24, 25].

In our previous work, Li_2GeO_3 in a binary Li_2O - GeO_2 system was reported to possess excellent dielectric properties with a relative permittivity $\epsilon_r \sim 6.36$, quality factor $Q \times f \sim 29\,000$ GHz, and a temperature coefficient of resonance frequency $\tau_f \sim -72$ ppm/ $^\circ\text{C}$ [26]. There are reasons to believe that by introducing B_2O_3 (melting point of $450\,^\circ\text{C}$) in the Li_2O - GeO_2 system, simultaneous low sintering temperature and good dielectric properties would be achieved [27]. Moreover, LiBGeO_4 is the only crystalline compound in the Li_2O - GeO_2 - B_2O_3 system, while the others are mainly non-crystalline (glassy), e.g. $\text{Li}_2\text{O} \cdot \text{B}_2\text{O}_3 \cdot \text{GeO}_2$ and $\text{Li}_2\text{O} \cdot \text{B}_2\text{O}_3 \cdot 4\text{GeO}_2$ [28], which makes it a unique material for LTCC application.

Single crystal LiBGeO_4 grown by a melting process was first reported by Ihara in 1971 [29], which followed subsequent studies on its crystal structure and nonlinear optical properties [30, 31]. However, despite its first reported synthesis was more than five decades ago, the main focus of research was on single crystal LiBGeO_4 . Synthesis of polycrystalline LiBGeO_4 has been challenging due to the volatility and hydrophilicity of boron resources [32]. Moreover, there has been a controversy regarding the crystal structure of LiBGeO_4 (orthorhombic or a tetragonal system), which results from the twinned structure of the single crystals [29, 33]. Therefore, the importance of the present work lies in the fact that the structure analysis based on ceramic powders will elude the twinned structure and provide reliable structure identification for LiBGeO_4 .

Moreover, the melting temperature (T_m) of LiBGeO_4 was reported to be around $900\,^\circ\text{C}$ [31], it is expected that LiBGeO_4 could be densified at relatively low temperatures ($\sim 600\,^\circ\text{C}$, $2/3T_m$), rendering its possible applications in ULTCC. Therefore, in the current work, trials for LiBGeO_4 ceramics via different processing routes were performed and the dielectric properties were

characterized over a broad frequency and temperature range.

2. Experimental

LiBGeO₄ ceramics were synthesized by a conventional solid-state reaction method, as reported in our previous work [2]. The raw materials were Li₂CO₃ (99.99%, Aladdin Industrial Corporation), GeO₂ (99.99%, Aladdin Industrial Corporation), and B₂O₃ (99.99%, Guo-Yao Co. Ltd, China). To obtain single-phase LiBGeO₄, three processes were proposed for powder synthesis: (i) Simple stoichiometric mixing of Li₂CO₃, B₂O₃, and GeO₂ in a ratio of 1:1:2; (ii) addition of extra 5 mol% B₂O₃ to compensate the loss of boron; (iii) Precursor synthesis: LiBO₂ powders were synthesized from Li₂CO₃ and B₂O₃ in a 1:1 ratio at 700 °C, as boron sources, which was subsequently mixed with GeO₂, and finally fired at 600-840 °C to form LiBGeO₄.

Thermoanalysis was done to guide chemical synthesis and ceramic densification using a DTA 499 F3 Jupiter (NETZSCH, Germany). The phase purity was investigated using an X-ray diffraction (XRD, CuK α 1, 1.54059Å, Model X' Pert PRO, PANalytical, Almelo, The Netherlands). The microstructures were examined using field-emission scanning electron microscopy (FESEM; S4800, Hitachi, Tokyo, Japan). The densities of all samples were measured by the Archimedes' method. Silver paste was coated on both sides of the ceramics and subsequently fired at 650 °C for 30 min. RF dielectric properties versus frequency and temperature were measured using an Agilent 4294A precision impedance analyzer and a TZDM-200-8001 MHz analyzer equipped with a temperature controller. The microwave dielectric properties were measured based on the modified Hakki-Coleman method [34, 35].

3. Results and discussion

3.1 Phase formation of LiBGeO₄

Based on the compositional design, three approaches were used to explore the formation of pure LiBGeO_4 . Figure 1 shows XRD pattern of the powder synthesized from simple mixing process at 820°C temperature. By indexing with the standard JCPDS card (No. 33-0792), the main phase was assigned to be LiBGeO_4 , but some peaks belonging to Li_2GeO_3 (No. 17-0193) were detected. 5mol% excess B_2O_3 addition, to some extent suppressed the formation of Li_2GeO_3 but did not eliminate the second phase. These results prove that a simple mixture of raw materials of Li_2CO_3 , B_2O_3 and GeO_2 failed to form single-phase LiBGeO_4 . This might be caused by the loss of B_2O_3 due to its solubility in the aqueous environment and volatilization during sintering at elevated temperatures.

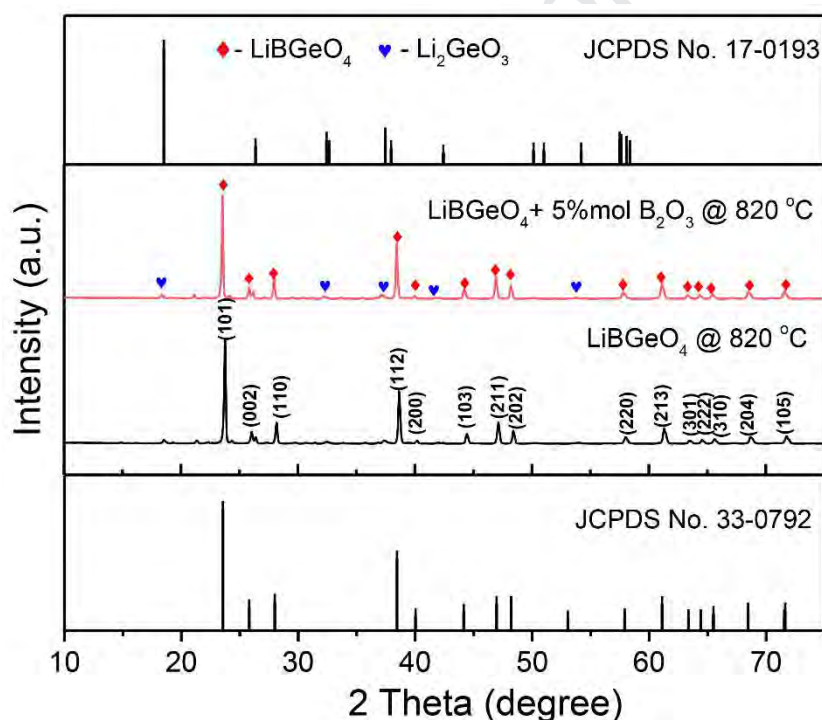


Figure 1 XRD patterns recorded on the calcined powders at 820°C from the simple mixing process: for the stoichiometric LiBGeO_4 and with 5 mol% extra B_2O_3 as raw materials and sintered (JCPDS No. 33-0792 for LiBGeO_4 , and No. 17-0193 for Li_2GeO_3).

Inspired by the precursor method to synthesize $\text{Pb}(\text{Mg}_{1/3}\text{Nb}_{2/3})\text{O}_3$ [36], B_2O_3 was pre-reacted with Li_2CO_3 to form LiBO_2 as a stable boron source, which was then reacted with GeO_2 to form LiBGeO_4 as shown in the following reaction sequence:

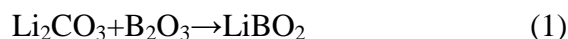




Figure S1 (in supplementary data) shows XRD pattern of the LiBO_2 powders calcined at 900°C , exhibiting a single phase by indexing with the JCPDF card No. 51-0517. To determine the thermodynamics of chemical reaction, thermal analysis was performed. Figure 2a shows the DSC curves of LiBO_2 and GeO_2 mixture in a 1:1 molar ratio in the temperature range of 25°C - 750°C . Two primary exothermic peaks were observed in that temperature range (495°C and $\sim 600^\circ\text{C}$). The first abroad peak can be attributed to the chemical reaction of the reactants while the second might be related to the transformation from the amorphous state to the crystalline state [37, 38]. A small peak $\sim 200^\circ\text{C}$, demonstrated the evaporation of hydroxide and/or residual water in the raw materials [39].

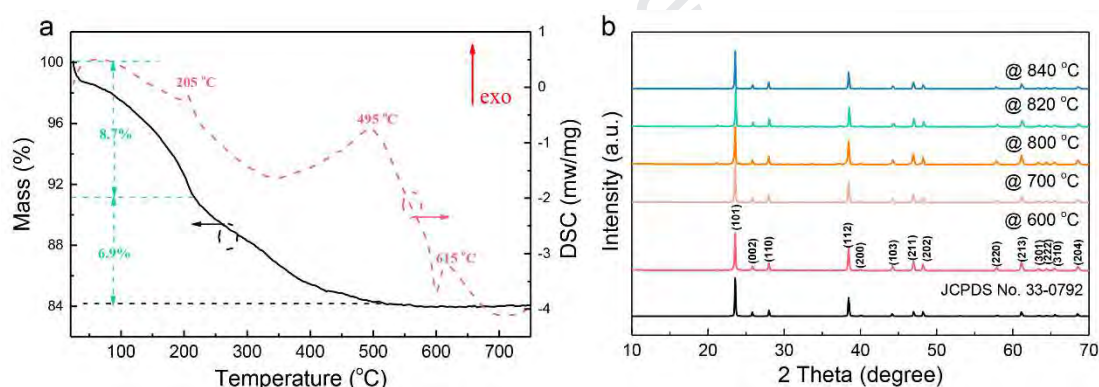


Figure 2 (a) Thermogravimetric analysis and differential scanning calorimeter (TGA/DSC) analysis of LiBGeO_4 ; (b) X-ray diffraction patterns of LiBGeO_4 sintered from 600 to 840°C .

Figure 2b shows X-ray diffraction patterns of as-sintered LiBGeO_4 at 600 - 840°C for 6 h from appropriate proportions of LiBO_2 and GeO_2 . Sharp diffraction peaks account for the high degree of crystallinity, which is in line with the DSC analysis. All peaks can be indexed to LiBGeO_4 (JCPDS No. 33-0792), which indicates the formation of LiBGeO_4 and its structural stability over a wide temperature range (600 - 840°C).

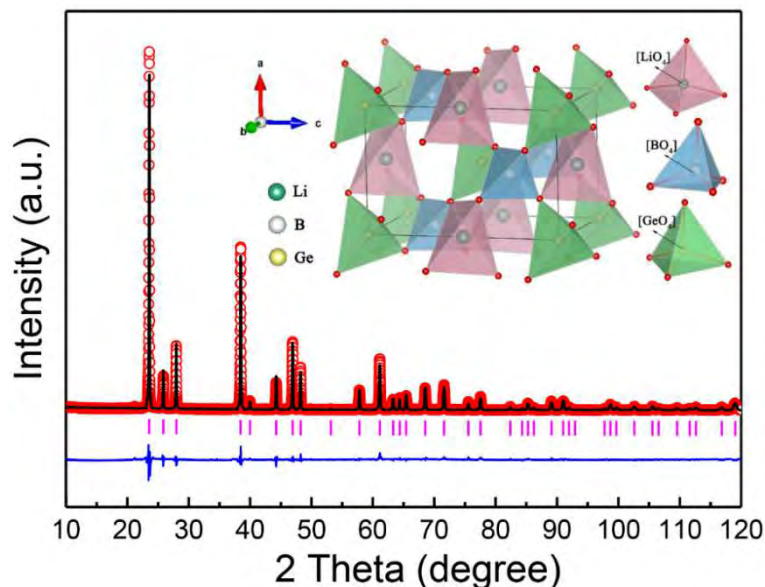


Figure 3 Rietveld refinement on the LiBGeO_4 sample via a two-step sintering at 820°C with the schematic crystal structure shown in the inset (the circle represents the calculated profiles, and the black line denotes the measured profiles, while the difference between them are shown in blue line; the pink lines denote the Bragg positions).

To further validate the phase purity and study the crystal structure of LiBGeO_4 , Rietveld refinement was performed using a structural model with an I-4 tetragonal structure based on the previous work [31]. The refinement was carried out in the order of the scale factor, zero shift, unit cell parameters, background polynomial, profile parameters, atomic positional coordinates, and isotropic temperature factors. A good match between the observed and the calculated patterns were obtained as shown in Figure 3 which indicates the valid structural model and the reliable refinement result. The schematic crystal structure and coordination polyhedron for Li, B and Ge are shown in the inset of Figure 3. The crystal structure is composed of alternating LiO_4 , BO_4 , and GeO_4 tetrahedra that are connected at corner to form frameworks. Each oxygen ion is coordinated by two Li^+ , one Ge^{4+} , and one B^{3+} ion. The Wyckoff position, atomic occupation, cell parameters, cell volume, Rietveld reliable factors R_p and R_{wp} are summarized in Table 1.

3.2 Microstructure evolution in LiBGeO_4

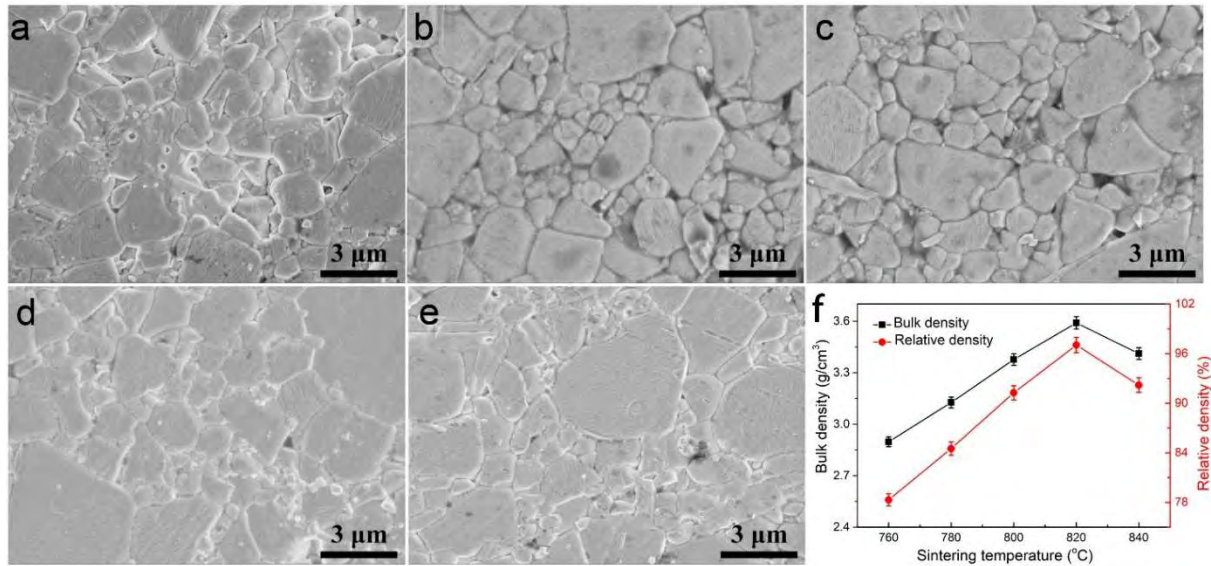


Figure 4 SEM images of LiBGeO₄ sintered at (a) 760 °C, (b) 780 °C, (c) 800 °C, (d) 820 °C, and (e) 840 °C, and (f) change in the bulk and relative densities of LiBGeO₄ as a function of sintering temperatures.

Figure 4 (a-e) shows the scanning electron micrographs for LiBGeO₄ samples sintered at various temperatures (760-840 °C). When sintered at 760 °C, the microstructure demonstrated largely closely packed grains, however, with a small amount of porosity (relative density ~ 78%). The grain size gradually increased with the increasing sintering temperature increased and a dense microstructure was achieved in the sample sintered at 820 °C (relative density ~ 97%).

3.3 Dielectric properties of LiBGeO₄

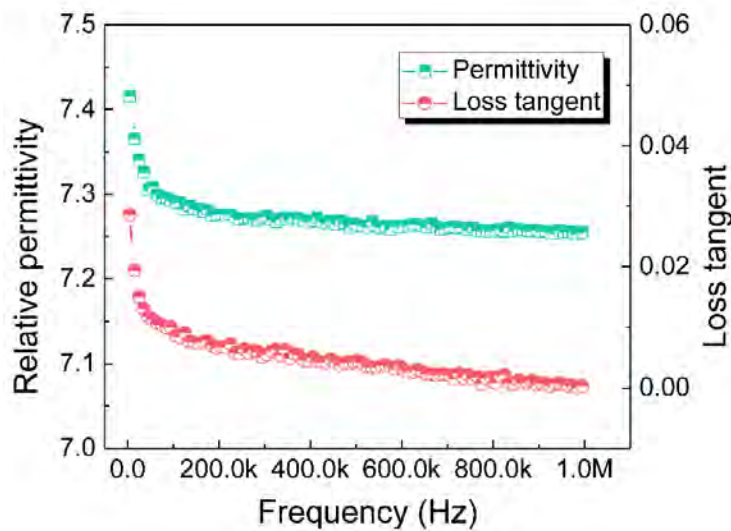


Figure 5 Frequency dependence of the relative permittivity and loss tangent recorded at radio frequencies from 100 Hz to 1 MHz.

Relative permittivity (ϵ_r) and dielectric loss tangent ($\tan\delta$) exhibited evident dependence on frequency, especially at low-frequency range with a steeper slope as shown in Figure 5. The dielectric constant decreases obviously when $f < 1$ kHz. Upon further increasing the frequency, ϵ_r reaches a stable value of 7.25. Similar trends were observed in loss tangent which decreases slightly with frequency. The frequency correlation of dielectric behaviors is attributed to the contribution to the polarization from slow mobile charges which cannot pace with the changing electric field at higher frequencies.

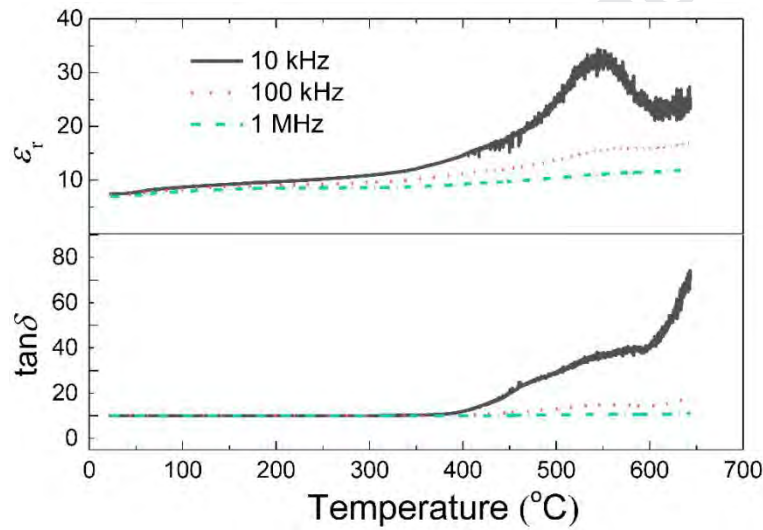


Figure 6 The temperature dependence of the relative permittivity and loss tangent of the LiBGeO₄ ceramics.

Figure 6 shows the variations in dielectric properties as a function of temperature in a broad range of 20-650 °C. Weak temperature dependence was observed at a lower temperatures (< 300 °C) which increased when temperature increased to 400 °C. During the same temperature range, the dielectric properties also exhibited frequency independence, with a strong temperature dependence on both ϵ_r and $\tan\delta$ occurring at $T > 400$ °C, accompanied by an obvious frequency dispersion. The increased dielectric constant, losses and frequency dispersion indicate the presence of one or more thermal activated polarizations that are frequency-dependent and frozen at low temperatures. Especially, the ϵ_r - T curve with $f = 10$ kHz shows a broad peak at 546 °C, which disappeared when the

frequency was increased to > 100 kHz. Combined with the remarkable decrease in the magnitudes of dielectric peaks and the nonpolar crystal space group (I-4), it is reasonable to refer that the observed dielectric anomaly is not related to a phase transition but a thermal-activated dielectric relaxation that is related to the space charges. Similar phenomena have also been reported in some ceramic materials, e.g. CaTiO_3 , $\text{Ca}_5\text{Nb}_4\text{TiO}_{17}$ [40, 41].

Space charges tend to aggregate at grain boundaries, which leads to electrically heterogeneous microstructures characterized by insulating grains and semiconducting grain boundaries. It is well known that impedance spectroscopy is a favorable technique to separate inhomogeneous microstructures by correlating the electrical properties to the microstructures [42-44]. Hence, to get a comprehensive understanding of the thermal activated dielectric anomaly, complex impedance analysis was conducted over the temperature range of 530 to 610 °C (the temperature range where dielectric anomaly occurred).

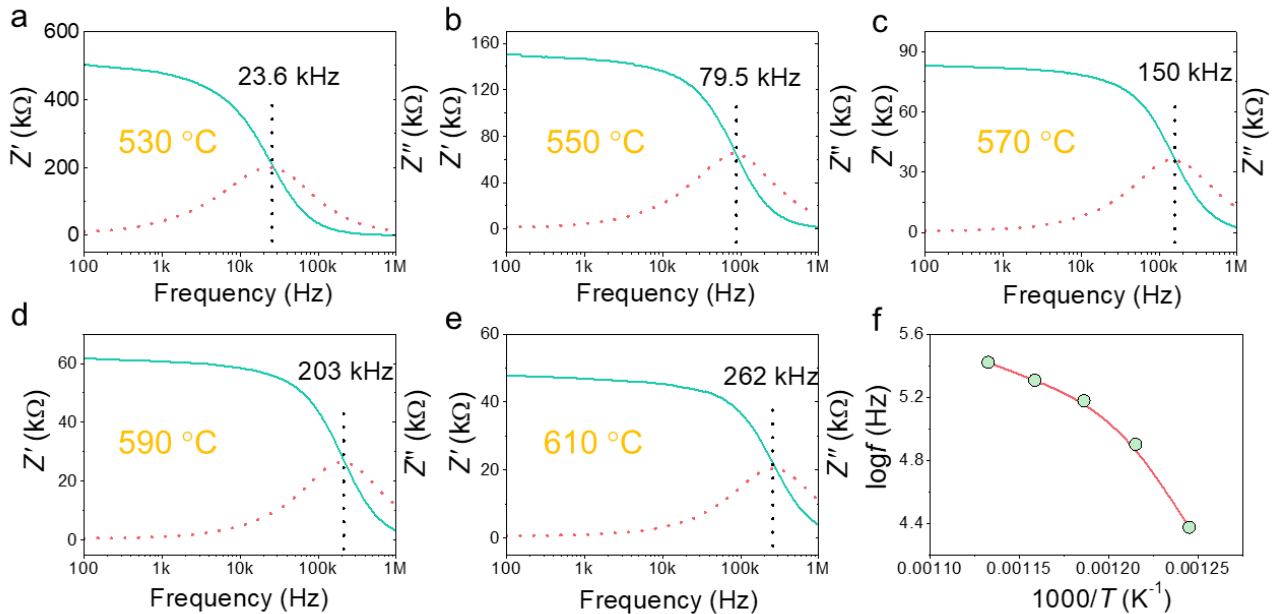


Figure 7 The frequency dependence of the real part (Z') and the imaginary part (Z'') of complex impedance at various temperatures (in log scale for the horizontal axis).

Figure 7 (a-e) shows the frequency dependence of the real part (Z') and the imaginary part (Z'') of impedance at various temperatures from 530-610 °C (in log scale). At a constant temperature, Z' value decreased continuously with increasing frequency. A sharp drop was observed at a characteristic frequency (also known as relaxation frequency f_r) at which the Z'' value reached the peak value. This characteristic frequency shifted f_r to a high-frequency band with increasing temperature, suggesting a thermally activated process. The variation in f_r (in log scale) is also plotted in Fig. 6f as a function of the reciprocal of temperature ($1/T$). Nonlinear variation is seen between $\log f$ and $1/T$ indicating that the correlated electrical relaxation is not a simple long-range conductivity but related to a variable-range-hopping electrical mechanism [45].

Table 2 summarizes the microwave dielectric properties (ϵ_r , $Q \times f$, and τ_f) of LiBGeO₄ sintered at various temperatures and compares the dielectric performances of some low-firing borates and germanates [13, 20, 24, 32, 46, 47]. For LiBGeO₄, both relative permittivity (ϵ_r) and quality factor ($Q \times f$) featured a strong dependence on sintering temperature with a rise-fall variation tendency; whereas the variation in τ_f with sintering temperature is low, and fluctuated around -90 ppm/°C. The sample sintered at 820 °C possessed a combination of optimized dielectric properties with $\epsilon_r = 6.28$, $Q \times f = 21,620$ GHz, and $\tau_f = -88.7$ ppm/°C. In comparison, the Li-based borates have a relatively low permittivity whereas Bi- and Ba-containing counterparts possess higher permittivities. As shown, either germanates or borates show negative τ_f values which need additional compensation mechanisms to modulate and satisfy practical needs. Generally, compositional regulation, either by forming composites or through ionic substitution to form solid solutions, has proved to be effective on compensating the τ_f values [48, 49]. Further efforts are in progress to adjust the thermal stability of resonance frequency for LiBGeO₄ via the addition of TiO₂ with $\tau_f = +450$ ppm/°C. Compared to

germanates, borates exhibit much lower sintering temperatures, making them a better potential candidate for application in LTCC or ULTCC technology.

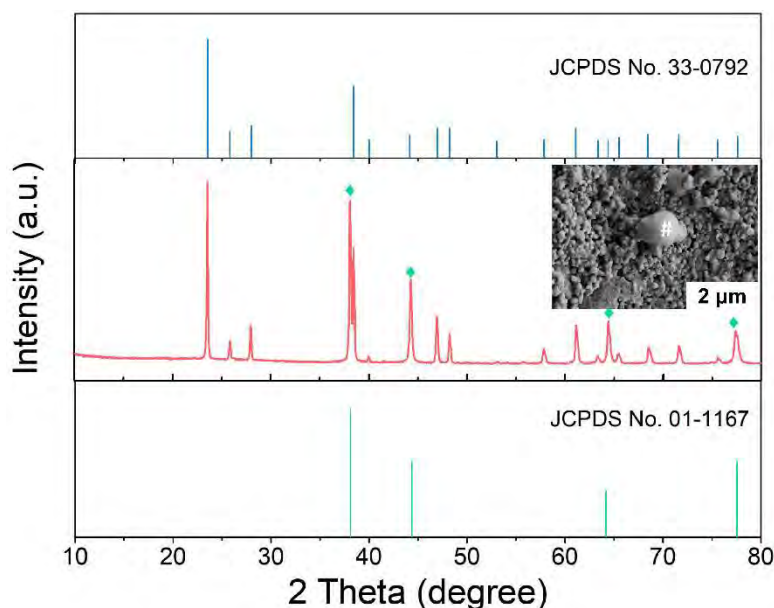


Figure 8 XRD and SEM micrograph of LiBGeO_4 cofired with silver electrode at 820 °C.

To estimate potential of LiBGeO_4 for practical application in LTCC, the sample was cofired with silver (Ag) electrode to determine the chemical compatibility as it is a vital part in LTCC technology. XRD was conducted on the cofired sample at 820 °C and shown in Figure 8. XRD exhibited separated diffraction peaks for Ag and LiBGeO_4 . Ag was indexed with a standard PDF cards (No. 01-1167). SEM images (in the inset of Figure 8) showed distinct grains which are different in sizes and elemental contrasts. These combination of XRD and SEM results indicate that no chemical reaction took place between LiBGeO_4 and silver, which is a convincing evidence for its utilization in LTCC technology.

4. Conclusions

Single-phase LiBGeO_4 ceramics were successfully prepared by a two-step process by which LiBO_2 was initially synthesized as a reliable boron resource followed by the synthesis of LiBGeO_4 powder. X-ray diffraction and Rietveld refinement confirmed that LiBGeO_4 crystallized in an I-4

tetragonal structure. Frequency and temperature had a dominant effect on dielectric properties above 400 °C. At 1 MHz, a low relative permittivity of 7.25 was obtained and at microwave frequency bands, the optimized dielectric properties with $\epsilon_r = 6.28$, $Q \times f = 21,620$ GHz, and $\tau_f = -88.7$ ppm/°C were achieved in the sample sintered at 820 °C. LiBGeO₄ also retain stable crystal structure when cofired with silver, which renders its capacity in low-temperature-cofiring ceramic technology. Our work provides a strategy for facile synthesis of phase pure borates, via the proposed two-step process to obtain stable boron resources.

Acknowledgments

C. Li gratefully acknowledges the financial support from the Natural Science Foundation of Guangxi Zhuang Autonomous Region (No. 2018GXNSFAA281253), and Z. Xing acknowledges the financial support from National Natural Science Foundation of Shaanxi (Grant No. 2019JQ-573), and Special Fund for high-level talents of Xijing University (No. XJ17T05).

References

- [1] Q.B. Lin, K.X. Song, B. Liu, H.B. Bafrooei, D. Zhou, W.T. Su, F. Shi, D.W. Wang, H.X. Lin, I.M. Reaney, Vibrational spectroscopy and microwave dielectric properties of $AY_2Si_3O_{10}$ ($A = Sr, Ba$) ceramics for 5G applications, *Ceram. Int.* 46 (2020) 1171-1177.
- [2] C.C. Li, H.C. Xiang, M.Y. Xu, Y. Tang, L. Fang, Li_2AGeO_4 ($A = Zn, Mg$): Two novel low-permittivity microwave dielectric ceramics with olivine structure, *J. Eur. Ceram. Soc.* 38 (2018) 1524-1528.
- [3] M.T. Sebastian, H. Jantunen, Low loss dielectric materials for LTCC applications: a review, *Int. Mater. Rev.* 53 (2008) 57-90.
- [4] D. Zhou, L.X. Pang, D.W. Wang, I.M. Reaney, Novel water-assisting low firing MoO_3 microwave dielectric ceramics, *J. Eur. Ceram. Soc.* 39 (2019) 2374-2378.
- [5] R. Umemura, H. Ogawa, H. Ohsato, A. Kan, A. Yokoi, Microwave dielectric properties of low-temperature sintered $Mg_3(VO_4)_2$ ceramic, *J. Eur. Ceram. Soc.* 25 (2005) 2865-2870.
- [6] G.G. Yao, P. Liu, X.G. Zhao, J.P. Zhou, H.W. Zhang, Low-temperature sintering and microwave dielectric properties of $Ca_5Co_4(VO_4)_6$ ceramics, *J. Eur. Ceram. Soc.* 34 (2014) 2983-2987.
- [7] C.C. Li, C.Z. Yin, J.Q. Chen, H.C. Xiang, Y. Tang, L. Fang, Crystal structure and dielectric properties of germanate melilites $Ba_2MGe_2O_7$ ($M = Mg$ and Zn) with low permittivity, *J. Eur. Ceram. Soc.*, 38 (2018) 5246-5251.
- [8] J.J. Bian, Y.F. Dong, New high Q microwave dielectric ceramics with rock salt structures: $(1-x)Li_2TiO_3+xMgO$ system ($0 \leq x \leq 0.5$), *J. Eur. Ceram. Soc.* 30 (2010) 325-330.
- [9] J.J. Bian, D.W. Kim, K.S. Kong, Glass-free LTCC microwave dielectric ceramics, *Mater. Res. Bull.* 40 (2005) 2120-2129.
- [10] D.W. Kim, K.S. Hong, C.S. Yoon, C.K. Kim, Low-temperature sintering and microwave dielectric properties of $Ba_5Nb_4O_{15}$ - $BaNb_2O_6$ mixtures for LTCC applications, *J. Eur. Ceram. Soc.* 23 (2003) 2597-2601.
- [11] G. Subodh, M.T. Sebastian. Glassfree $Zn_2Te_3O_8$ microwave ceramic for LTCC applications, *J. Am. Ceram. Soc.* 90 (2007) 2266-2268.
- [12] P.S. Anjana, M.T. Sebastian, Microwave dielectric properties and low-temperature sintering of cerium oxide for LTCC applications, *J. Am. Ceram.* 92 (2009) 96-104.

- [13] L.H. Ouyang, W.Q. Wang, H.C. Fan, Z.Z. Weng, W.W. Wang, H. Xue, Sintering behavior and microwave performance of CaSiO_3 ceramics doped with $\text{BaCu}(\text{B}_2\text{O}_5)$ for LTCC applications, *Ceram. Int.* 45 (2019) 18937-18942.
- [14] A. Borisevich, P.K. Davies, Microwave dielectric properties of $\text{Li}_{1+x-y}\text{M}_{1-x-3y}\text{Ti}_{x+4y}\text{O}_3$ ($\text{M} = \text{Nb}^{5+}$, Ta^{5+}) solid solutions, *J. Eur. Ceram. Soc.* 21 (2001) 1719-1722.
- [15] M. Udovic, M. Valant, D. Suvorov, Phase formation and dielectric characterization of the Bi_2O_3 - TeO_2 system prepared in an oxygen atmosphere, *J. Am. Ceram. Soc.* 87 (2004) 591-597.
- [16] M.T. Sebastian, *Dielectric Materials for Wireless Communications*, Elsevier (2008).
- [17] M.T. Sebastian, H. Wang, H. Jantunen, Low temperature co-fired ceramics with ultra-low sintering temperature: A review, *Curr. Opin. Solid State Mater. Sci.* 20 (2016) 151-170.
- [18] K.G. Wang, H.F. Zhou, X.B. Liu, W.D. Sun, X.L. Chen, H. Ruan, A lithium aluminum borate composite microwave dielectric ceramic with low permittivity, near-zero shrinkage, and low sintering temperature, *J. Eur. Ceram. Soc.* 39 (2019) 1122-1126.
- [19] Y.J. Seo, J.S. Dong, S.C. Yong, Phase evolution and microwave dielectric properties of lanthanum borate-based low-temperature Co-fired ceramics materials. *J. Am. Ceram. Soc.* 89 (2006) 2352-2355.
- [20] X. Chen, W. Zhang, B. Zalinska, I. Sterianou, S. Bai, I.M. Reaney, Low sintering temperature microwave dielectric ceramics and composites based on Bi_2O_3 - B_2O_3 , *J. Am. Ceram. Soc.* 95 (2012) 3207-3213.
- [21] D. Zhou, L.X. Pang, J. Guo, Z.M. Qi, T. Shao, Q.P. Wang, H.D. Xie, X. Yao, C.A. Randall, Influence of Ce substitution for Bi in BiVO_4 and the impact on the phase evolution and microwave dielectric properties, *Inorg. Chem.* 53 (2014) 1048-1055.
- [22] H.R. Zheng, S.H. Yu, L.X. Li, X.S. Lyu, Z. Sun, S.L. Chen, Crystal structure, mixture behavior, and microwave dielectric properties of novel temperature stable $(1-x)\text{MgMoO}_4$ - $x\text{TiO}_2$ composite ceramics, *J. Eur. Ceram. Soc.* 37 (2017) 4661-4665.
- [23] H.C. Xiang, C.C. Li, Y. Tang, L. Fang, Two novel ultralow temperature firing microwave dielectric ceramics LiMVO_6 ($\text{M} = \text{Mo}, \text{W}$) and their chemical compatibility with metal electrodes, *J. Eur. Ceram. Soc.* 37 (2017) 3959-3963.
- [24] M. Ohashi, H. Ogawa, A. Kan, E. Tanaka, Microwave dielectric properties of low-temperature sintered $\text{Li}_3\text{AlB}_2\text{O}_6$ ceramic, *J. Eur. Ceram. Soc.* 25 (2005) 2877-2881.

- [25] W.B. Hong, L. Li, H. Yan, S.Y. Wu, H.S. Yang, X.M. Chen, Room-temperature-densified H_3BO_3 microwave dielectric ceramics with ultra-low permittivity and ultra-high $Q \times f$ value, *J. Materiomics* 6 (2020) 233-239.
- [26] C.Z. Yin, H.C. Xiang, C.C. Li, H. Porwal, L. Fang, Low-temperature sintering and thermal stability of Li_2GeO_3 -based microwave dielectric ceramics with low permittivity, *J. Am. Ceram. Soc.* 101 (2018) 4608-4614.
- [27] L. Li, C.H. Liu, J.Y. Zhu, X.M. Chen, B_2O_3 -modified fused silica microwave dielectric materials with ultra-low dielectric constant, *J. Eur. Ceram. Soc.* 35 (2015) 1799-1805.
- [28] K. Błaszczak, A. Adamczyk, M. Wędzikowska, M. Rokita, Infrared studies of devitrification $\text{Li}_2\text{O-B}_2\text{O}_3\text{-2GeO}_2$ glass, *J. Mol. Struct.* 704 (2004) 275-279.
- [29] M. Ihara, The crystal structure of lithium borogermanate, $\text{Li}_2\text{O-B}_2\text{O}_3\text{-(GeO}_2)_2$, Japan: *J. Ceram. Assoc.* 79 (1971) 152-155.
- [30] Y. Takahashi, Y. Benino, T. Fujiwara, T. Komatsu, Second-order optical nonlinearity of LaBGeO_5 , LiBGeO_4 and $\text{Ba}_2\text{TiGe}_2\text{O}_8$ crystals in corresponding crystallized glasses, *Jpn. J. Appl. Phys.* 41 (2002) 1455-1458.
- [31] J. Parise, T.J.C.O.M. Gier, Hydrothermal syntheses and structural refinements of single crystal lithium boron germanate and silicate, LiBGeO_4 and LiBSiO_4 , *Chem. Mater.* 4 (1992) 1065-1067.
- [32] D. Zhou, L.X. Pang, D.W. Wang, Z.M. Qi, I.M. Reaney, High quality factor, ultralow sintering temperature $\text{Li}_6\text{B}_4\text{O}_9$ microwave dielectric ceramics with ultralow density for antenna substrates, *ACS Sustainable Chem. Eng.* 6 (2018) 11138-11143.
- [33] A. Rulmont, P. Tarte, J.M. Winand, Vibrational spectrum of crystalline and glassy LiBGeO_4 : structural analogies with BaSO_4 , *J. Mater. Sci. Lett.* 6 (1987) 659-662.
- [34] B. W. Hakki, P. D. Coleman. A dielectric resonator method of measuring inductive capacities in the millimeter range. *IRE Trans. Microw. Theory Tech.* MTT-8 (1960) 402-410.
- [35] W. E. Courtney. Analysis and evaluation of a method of measuring complex permittivity and permeability of microwave materials. *IEEE Trans. Microw. Theory Tech.* MTT-18(1970) 476-485.
- [36] S.L. Swartz, T.R. Shrout, Fabrication of perovskite lead magnesium niobate, *Mater. Res. Bull.* 17 (1982) 1245-1250.
- [37] H.C. Xiang, Y. Bai, C.C. Li, L. Fang, Structural, thermal and microwave dielectric properties of

- the novel microwave material $\text{Ba}_2\text{TiGe}_2\text{O}_8$, *Ceram. Int.* 44 (2018) 10824-10828.
- [38] M.I. Diaz-Guemes, A.S. Bhatti, D. Dollimore, The thermal decomposition of oxalates: Part 22. The preparation and thermal decomposition of some oxy tungsten (VI) oxalates, *Thermochim. Acta* 111 (1987) 275-282.
- [39] C.C. Li, C.Z. Yin, M. Deng, L.L. Shu, J. Khaliq, Tunable microwave dielectric properties in $\text{SrO-V}_2\text{O}_5$ system through compositional modulation, *J. Am. Ceram. Soc.* 103 (2020) 2315-2321.
- [40] V.V. Lemanov, A.V. Sotnikov, E.P. Smirnova, M. Weihnacht, R. Kunze, Perovskite CaTiO_3 as an incipient ferroelectric, *Solid State Commun.* 110 (1999) 611-614.
- [41] C.C. Li, X.Y. Wei, L. Fang, H.X. Yan, M.J. Reece, Dielectric relaxation and electrical conductivity in $\text{Ca}_5\text{Nb}_4\text{TiO}_{17}$ ceramics, *Ceram. Int.* 41 (2015) 9923-9930.
- [42] J.T.S. Irvine, D.C. Sinclair, A.R. West, Electroceramics: characterization by impedance spectroscopy, *Adv. Mater.* 2 (1990) 132.
- [43] C.C. Li, X.Y. Wei, L. Fang, Dielectric and complex impedance analysis of $\text{Sr}_3\text{Nb}_4\text{TiO}_{17}$ ceramic with perovskite-like structure, *J Mater Sci: Mater Electron* 26 (2015) 8714-8719.
- [44] C.C. Li, H.C. Xiang, J.W. Chen, L. Fang, Phase transition, dielectric relaxation and piezoelectric properties of bismuth doped $\text{La}_2\text{Ti}_2\text{O}_7$ ceramics, *Ceram. Int.* 42 (2016) 11453-11458.
- [45] A.K. Jonscher. Dielectric relaxation in solids, *J. Phys. D: Appl. Phys.* 14 (1999) 57-70.
- [46] X.H. Ma, S.H. Kweon, S. Nahm, C.Y. Kang, S.J. Yoon, Y.S. Kim, Synthesis and microwave dielectric properties of $\text{Bi}_2\text{Ge}_3\text{O}_9$ ceramics for application as advanced ceramic substrate, *J. Eur. Ceram. Soc.* 37 (2017) 605-610.
- [47] H. Luo, L. Fang, H.C. Xiang, Y. Tang, C.C. Li, Two novel low-firing germanates $\text{Li}_2\text{MGe}_3\text{O}_8$ (M = Ni, Co) microwave dielectric ceramics with spinel structure, *Ceram. Int.* 43 (2017) 1622-1627.
- [48] X.K. Lan, Z.Y. Zou, W.Z. Lu, J.H. Zhu, W. Lei, Phase transition and low-temperature sintering of $\text{Zn}(\text{Mn}_{1-x}\text{Al}_x)_2\text{O}_4$ ceramics for LTCC applications. *Ceramics International*, 2016, 42(15): 17731-17735.

- [49] Y.H. Zhang, H.T. Wu, Crystal structure and microwave dielectric properties of $\text{La}_2(\text{Zr}_{1-x}\text{Ti}_x)_3(\text{MoO}_4)_9$ ($0 \leq x \leq 0.1$) ceramics, J. Am. Ceram. Soc., 102 (2019), 4092-4102.

Table 1 The Wyckoff position, atomic occupation, cell parameters, cell volume, and Rietveld reliable factors R_p and R_{wp}

Atom	Wyckoff	x	y	z	Occ.
Li1	2b	0.000	0.000	0.500	1.000
Ge1	2a	0.000	0.000	0.000	1.000
B1	2c	0.000	0.500	0.250	1.000
O1	8g	0.178	0.300	0.135	1.000
$a = b = 4.508 \text{ \AA}$, $V = 139.9 \text{ \AA}^3$, $R_p = 7.47\%$, $R_{wp} = 9.82\%$					

Table 2 Sintering temperature and microwave dielectric properties of LiBGeO₄ compared with some low-firing borates and germanates.

Compound	S.T. (°C)	ϵ_r	$Q \times f$ (GHz)	τ_f (ppm/°C)	electrode	Reference
LiBGeO ₄	760	6.17	17,490	-94.1	Ag	This work
	780	6.22	18,900	-89.2		
	800	6.25	20,980	-92.0		
	820	6.28	21,620	-88.7		
	840	6.20	19,760	-86.3		
BaCu(B ₂ O ₅)	810	7.4	50,000	-32	not studied	[13]
Bi ₆ B ₁₀ O ₂₄	660	10	10,800	-41	not studied	[20]
Bi ₄ B ₂ O ₉	625	39	2600	-203	not studied	[20]
Li ₃ AlB ₂ O ₆	640	6.0	41,800	-72	not studied	[24]
Li ₆ B ₄ O ₉	640	5.95	41,800	-72	Ag	[32]
Bi ₂ Ge ₃ O ₉	875	9.7	48,573	-29.5	not studied	[46]
Li ₂ NiGe ₃ O ₈	940	8.6	42,200	-78.2	Ag	[47]
Li ₂ CoGe ₃ O ₈	950	9.0	40,500	-42	Ag	[47]

Figure captions:

Figure 1 XRD patterns for stoichiometric LiBGeO_4 and $\text{LiB}_{1.05}\text{GeO}_4$ with B_2O_3 and H_3BO_3 as raw materials and sintered at 820 °C.

Figure 2 (a) Thermogravimetric analysis and differential scanning calorimeter (TGA/DSC) analysis of LiBGeO_4 ; (b) X-ray diffraction patterns of LiBGeO_4 sintered from 600 to 840 °C.

Figure 3 Rietveld refinement on the LiBGeO_4 sample via a two-step sintering at 820 °C with the schematic crystal structure shown in the inset.

Figure 4 SEM images of LiBGeO_4 sintered at (a) 760 °C, (b) 780 °C, (c) 800 °C, (d) 820 °C, and (e) 840 °C, and (f) change in the bulk and relative densities of LiBGeO_4 as a function of sintering temperatures.

Figure 5 The frequency dependence of the relative permittivity and loss tangent recorded at radio frequencies from 100 Hz to 1 MHz.

Figure 6 The temperature dependence of the relative permittivity and loss tangent of the LiBGeO_4 ceramics.

Figure 7 The frequency dependence of the real part (Z') and the imaginary part (Z'') of complex impedance at various temperatures (in log scale for the horizontal axis).

Figure 8 (a) XRD and (b) SEM micrograph of LiBGeO_4 cofired with silver electrode at 820 °C.

Declaration of interests

☒ The authors declare that they have no known competing financial interests or personal relationships that could have appeared to influence the work reported in this paper.

☐ The authors declare the following financial interests/personal relationships which may be considered as potential competing interests: